www.nature.com/aps

Acta Pharmacologica Sinica

ARTICLE

A novel resveratrol analog upregulates sirtuin 1 and inhibits inflammatory cell infiltration in acute pancreatitis

Zheng-nan Ren[1,2], Jun Yang[3], Meng-ya Zhang[1,2], Yi-wen Huang[1,2], Dong-xiao Song[1,2], Xun Sun[4], Li-long Pan[1] and Jia Sun[1,2]

Acute pancreatitis (AP), an inflammatory disorder of the pancreas, is a complicated disease without specific drug therapy. (*R*)-4,6-dimethoxy-3-(4-methoxy phenyl)-2,3-dihydro-1H-indanone [(*R*)-TML104] is a synthesized analog of the natural product resveratrol sesquiterpenes (±) -isopaucifloral F. This study aimed to investigate the effect and underlying mechanism of (*R*)-TML104 on AP. The experimental AP model was induced by caerulein hyperstimulation in BALB/c mice. (*R*)-TML104 markedly attenuated caerulein-induced AP, as evidenced by decreased pancreatic edema, serum amylase levels, serum lipase levels, and pancreatic myeloperoxidase activity. In addition, (*R*)-TML104 significantly inhibited the expression of pancreatic chemokines C–C motif chemokine ligand 2 and macrophage inflammatory protein-2 and the infiltration of neutrophils and macrophages. Mechanistically, (*R*)-TML104 activated AMP-activated protein kinase and induced sirtuin 1 (SIRT1) expression. (*R*)-TML104 treatment markedly induced the SIRT1-signal transducer and activator of transcription 3 (STAT3) interaction and reduced acetylation of STAT3, thus inhibiting the inflammatory response mediated by the interleukin 6-STAT3 pathway. The effect of (*R*)-TML104 on SIRT1-STAT3 interaction was reversed by treatment with a SIRT1 inhibitor selisistat (EX527). Together, our findings indicate that (*R*)-TML104 alleviates experimental pancreatitis by reducing the infiltration of inflammatory cells through modulating SIRT1.

Keywords: acute pancreatitis; resveratrol analog; sirtuin 1; signal transducer and activator of transcription 3; anti-inflammation

Acta Pharmacologica Sinica (2022) 43:1264–1273; https://doi.org/10.1038/s41401-021-00744-y

INTRODUCTION

Acute pancreatitis (AP) is a trypsin-activated sudden inflammatory response in the pancreas, that is initiated by various etiological factors, causing autodigestion of the pancreas [1–5]. It is a potentially life-threatening disease characterized by tissue edema, necrosis, and hemorrhage in the pancreas. The cellular pathophysiology of AP remains incompletely understood. Currently, specific drug treatment is unavailable for AP [6]. Infiltration of innate immune cells (neutrophils, macrophages, and other cells) potentiates the pancreatic inflammatory response, which closely correlates with the development and severity of AP [7, 8]. The chemokines C–C motif chemokine ligand 2 (CCL2) and macrophage inflammatory protein-2 (MIP-2) are key mediators of increased neutrophil and macrophage recruitment in damaged organs, respectively [5, 9–12]. Interleukin-6 (IL-6) plays a critical role in the activation of signal transducer and activator of transcription 3 (STAT3), a key transcription factor associated with mediating the expression of chemokines, including CCL2 and MIP-2 [13]. The activation of STAT3 via IL-6 trans-signaling has also been shown to mediate severe AP and pancreatitis-associated uncontrolled systemic inflammatory responses [14, 15]. Interestingly, inhibition of STAT3 acetylation impairs its phosphorylation and transcriptional function [16]. Inhibition of STAT3 activity by suppressing its acetylation may be a potential strategy to alleviate AP progression.

Resveratrol (3,4′,5-trihydroxystilbene), a plant polyphenol, is a naturally occurring substance present in a variety of plant species. It possesses cardioprotective, anticancer, antioxidant, and anti-inflammatory properties via the upregulation of sirtuin 1 (SIRT1) [17–19]. Resveratrol has been indicated to relieve AP and is related to the enhancement of SIRT1-mediated deacetylation [20]. Although the protective effect of resveratrol on AP has been reported [21–23], extensive metabolism in the intestine and liver results in its bioavailability of less than 1% [24, 25]. Moreover, dose-escalation or repeated administration of resveratrol could not overcome this problem [24]. Thus, structural modification of resveratrol is needed to increase systemic bioavailability and metabolic stability, thus persevering its beneficial function. Here, we evaluated the protective effect

[1]Wuxi Medical School and School of Food Science and Technology, Jiangnan University, Wuxi 214122, China; [2]State Key Laboratory of Food Science and Technology, Jiangnan University, Wuxi 214122, China; [3]Department of General Surgery, Affiliated Hospital of Jiangnan University, Wuxi 214122, China and [4]Department of Natural Products Chemistry, School of Pharmacy, Fudan University, Shanghai 201203, China
Correspondence: Xun Sun (sunxunf@shmu.edu.cn) or Li-long Pan (llpan@jiangnan.edu.cn) or Jia Sun (jiasun@jiangnan.edu.cn)
These authors contributed equally: Zheng-nan Ren, Jun Yang, Meng-ya Zhang

Received: 5 March 2021 Accepted: 12 July 2021
Published online: 6 August 2021

and underlying mechanism of a structurally optimized analog of the natural product resveratrol sesquiterpenes (±) -isopaucifloral F, (*R*)-4,6-dimethoxy-3-(4-methoxy phenyl)-2,3-dihydro-1H-indanone [(*R*)-TML104], on experimental AP.

MATERIALS AND METHODS

Chemicals and antibodies

Caerulein and pentobarbital sodium were purchased from Sigma-Aldrich (Shanghai, China). Resveratrol was purchased from Aladdin (Shanghai, China). (*R*)-TML104 was synthesized and provided by Prof. Xun Sun's laboratory in the School of Pharmacy (Fudan University, Shanghai, China). SIRT1 inhibitor selisistat (EX527) was purchased from Meilunbio (Liaoning, China). Antibodies against SIRT1 (ab189494), Ly6G (ab25377), and CD68 (ab955) were purchased from Abcam (Shanghai, China). Antibodies for p-STAT3 (AP0705), p-AMPK (AP1002), AMPK (A1229), β-Actin (AC026), pan Acetyl-lysine (A2391), and CCL2 (A7277) were purchased from Abclonal (Hubei, China). Antibodies for MIP-2 (26791-1-AP) and STAT3 (10253-2-AP) were purchased from Proteintech (Hubei, China). Alexa Fluor 488 goat anti-rat IgG (H + L) cross-adsorbed secondary antibody (A-11006), Alexa Fluor 594 goat anti-mouse IgG (H + L) highly cross-adsorbed secondary antibody (A-11032), and Alexa Fluor 594 goat anti-rabbit IgG (H + L) highly cross-adsorbed secondary antibody (A-11037) were purchased from Invitrogen (CA, USA). 4′,6-Diamidino-2-phenylindole (DAPI) was purchased from Solarbio (Beijing, China). Collagenase-P was purchased from Roche (Basel-Stadt, Switzerland). The following antibodies were used for flow cytometry: PE/Cyanine7 anti-mouse CD45 (103114), Brilliant Violet 421™ anti-mouse F4/80 (123132), Alexa Fluor 488 anti-mouse CD206 (MMR) (141710), and Brilliant Violet 421™ anti-mouse Ly-6G (127628) from Biolegend (CA, USA), APC anti-mouse CD11b from BD Biosciences (561690; NJ, USA) and PE anti-mouse iNOS from eBioscience (12-5920-80; MA, USA).

Mice

BALB/c mice (7–8 weeks old, 20 ± 2 g) were purchased from JOINN Laboratories (Jiangsu, China) and maintained in a specific pathogen-free environment at the Wuxi Medical School Experimental Animal Center of Jiangnan University (Jiangsu, China) with controlled temperature (24 ± 1 °C), 12–12 h light-dark cycle, and free water and standard chow (AIN93G; Xietong Pharmaceutical Bio-engineering Co., Ltd, Jiangsu, China). All mice were adjusted to laboratory conditions 1 week before the experiments and fasted for 12 h before induction of AP. All experimental procedures involving mice were carried out according to protocols approved by the Institutional Animal Ethics Committee of Jiangnan University (JN. No. 20190915c0401020[204]). Animal studies were reported in compliance with the ARRIVE guidelines [26].

Experimental design and animal treatments

Experimental AP was induced by caerulein as described in our previous studies [12, 27]. BALB/c mice were divided randomly into the following experimental groups ($n = 6$–10): saline-treated control group (CON), (*R*)-TML104-only-treated group [(*R*)-TML104], caerulein-induced AP group (CAE), (*R*)-TML104 prophylactic group [(*R*)-TML104 + CAE], resveratrol prophylactic group (Res + CAE), and SIRT1 inhibitor-treated group [(*R*)-TML104 + EX527 + CAE]. All animals were given hourly intraperitoneal injections of normal saline or saline-containing caerulein (50 μg· kg^{-1}) for 8 h. Resveratrol (20 mg· kg^{-1}) [28] and (*R*)-TML104 (5, 10 and 20 mg· kg^{-1}) were intraperitoneally administered 2 h before caerulein stimulation. EX527 (20 mg· kg^{-1}) [29] was intraperitoneally infused 0.5 h before the first caerulein injection. For the vehicle control, the CON, and CAE groups were administered with saline 0.5 h before the first caerulein challenge. One hour after the last caerulein injection, mice were sacrificed by administering a lethal dose of pentobarbital sodium. Blood and pancreatic tissue samples were harvested for subsequent assays.

Determination of pancreatic edema

The edema of the pancreas was quantified by the ratio of wet weight to dry weight. The initial weight of the freshly harvested pancreas was defined as wet weight. The weight of the same sample after desiccation at 60 °C for 72 h was determined as dry weight.

Measurement of amylase, lipase, and myeloperoxidase (MPO) activities

Fresh blood was collected and centrifuged at 3000×*g* for 15 min at room temperature. The supernatant was then collected and stored at −80 °C until analysis. Serum amylase activity was determined using an iodine-starch colorimetric assay kit (C016-1-1; Jiancheng Bioengineering Institute, Jiangsu, China). Serum lipase activity was measured using a colorimetric assay kit (A054-1-1; Jiancheng Bioengineering Institute). Pancreatic MPO activity was evaluated using a myeloperoxidase assay kit (A044-1-1; Jiancheng Bioengineering Institute) according to the protocol of the manufacturer.

Histopathological analyses

Fresh pancreatic samples were collected and fixed in 4% buffered formalin for 36 h at 4 °C, embedded in paraffin, and sliced using Skiving Machine Slicer (RM2245; Leica, Wetzlar, Germany). The 5 μm slices were stained with hematoxylin and eosin (H&E) following the standard procedure. For pancreatic morphology evaluation, a digital slice scanner (Pannoramic MIDI; 3DHISTCH, Budapest, Hungary) was used.

Enzyme-linked immunosorbent assays (ELISA)

Pancreatic IL-6, CCL2, and MIP-2 levels were measured with ELISA kits from Sbjbio (SBJ-M0044, SBJ-M0936, and SBJ-M0269; Jiangsu, China) according to the protocols of the manufacturer. Absorbance was measured at 450 nm with a microplate reader Multiclan GO (Thermos Fisher Scientific Inc, MA, USA). Pancreatic tissue samples were homogenized in a saline solution (1:19, *w*/*v*) using a homogenizer (Scientz-48; Polytron, Zhejiang, China) at 55 Hz for 1 min. Samples were centrifuged at 4 °C, 10,000×*g* for 10 min. Protein concentrations were determined by BCA Protein Assay Kit (P0010; Beyotime, Shanghai, China) during sample preparation to ensure that an equal quantity of protein was applied for cytokine measurements.

Immunoblotting

Pancreatic samples were homogenized in ice-cold lysis buffer RIPA (P0013B; Beyotime; containing protease inhibitors and phosphatase inhibitors). Protein concentrations were determined by using a BCA Protein Assay Kit. Equal amounts of protein were electrophoretically separated in sodium dodecyl sulfate (SDS)-polyacrylamide gels and then transferred onto nitrocellulose filter membranes (Merck, Shanghai, China). The membranes were blocked with 5% *w*/*v* non-fat dry milk in TBS-Tween 20 for 1 h at room temperature, further incubated with appropriately diluted primary antibodies overnight at 4 °C, and probed with secondary peroxidase-labeled antibody for 2 h at room temperature. The dilution ratios of primary antibodies were as follows: STAT3 (1:4000), SIRT1 (1:1000), p-STAT3 (1:1000), p-AMPK (1:1000), AMPK (1:1000), and β-Actin (1:200,000). The protein blots were visualized by

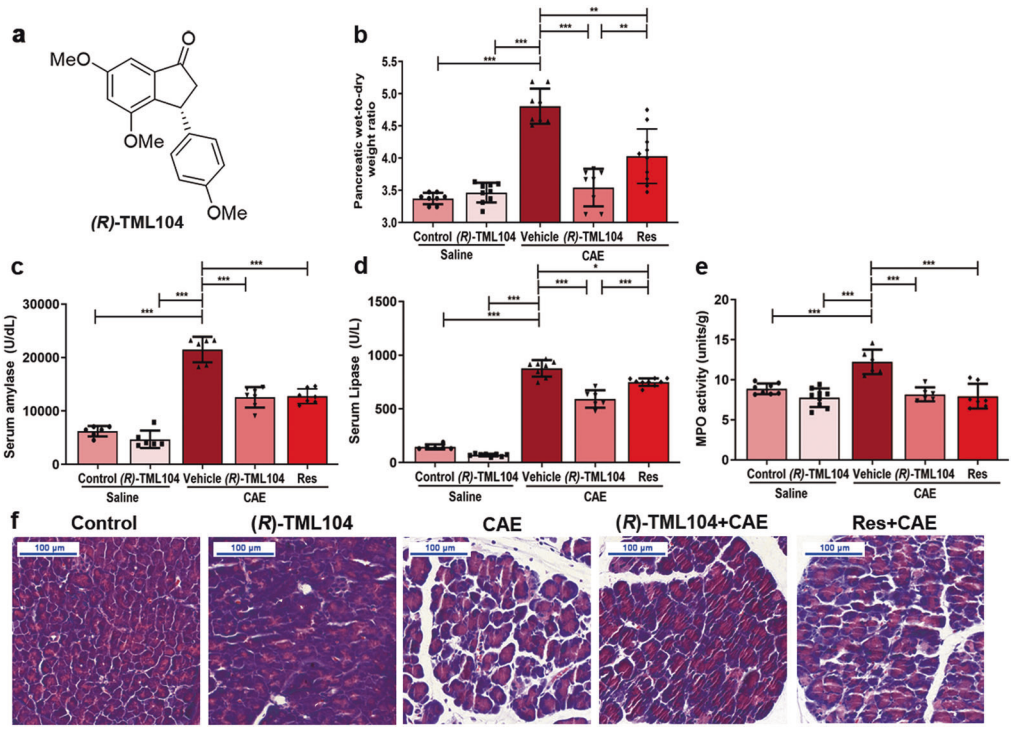

Fig. 1 (*R*)-TML104 mitigates pancreatic damage in caerulein-induced AP. a Chemical structure of (*R*)-TML104. **b** Pancreatic wet-to-dry weight ratio. **c** Serum amylase levels. **d** Serum lipase levels. **e** Pancreatic MPO activities. **f** Representative images of pancreatic damage by H&E staining. Scale bar: 100 μm. Data (**b**)–(**e**) were mean ± SD ($n = 6$–10). Data (**f**) were representative of six independent mice. $^{*}P < 0.05$, $^{**}P < 0.01$, $^{***}P < 0.001$.

plus-enhanced chemiluminescence using ChemiDoc Imager (Bio-Rad, CA, USA). The densitometric analyses of protein expression were performed by AlphaView Software (ProteinSimple, CA, USA).

Immunofluorescence

Five-μm slices were cut from paraffin-embedded blocks and placed on microscope slides. Antigen retrieval was performed for 30 min. After blocking with bovine serum albumin (1%) for 1 h, the slides were incubated overnight at 4 °C with antibodies against Ly6G (1:200), CD68 (1:100), CCL2 (1:100) or MIP-2 (1:100). The slides were washed with PBS and incubated for 1.5 h at room temperature with Alexa Fluor 488 goat anti-rat IgG (H + L) cross-adsorbed secondary antibody, Alexa Fluor 594 goat anti-mouse IgG (H + L) highly cross-adsorbed secondary antibody, or Alexa Fluor 594 goat anti-rabbit IgG (H + L) highly cross-adsorbed secondary antibody (all in 1:200). Nuclei were counterstained with DAPI. The slides for immunofluorescence staining were examined using microscopy (Vert A1, Carl Zeiss, Baden-Württemberg, Germany).

Flow cytometry

Freshly harvested pancreatic tissue samples were digested in 0.75 mg·mL^{-1} collagenase-P solution at 37 °C for 15 min. Subsequently, tissue was homogenized in gentleMACS^{TM} Dissociators (Miltenyi Biotec, Nordrhein-Westfalen, Germany) and filtered through the 75 μm filter screen with phosphate buffer saline (PBS). Single-cell suspensions were incubated for 15 min at room temperature in PBS with the antibodies. Gating methods of fluorescence-activated cell sorting were programmed as $CD45^{+}CD11b^{+}Ly6G^{+}$ for neutrophils, $CD45^{+}CD11b^{+}F4/80^{+}$ for macrophages, $CD45^{+}CD11b^{+}F4/80^{+}iNOS^{+}CD206^{-}$ for M1 macrophages, and $CD45^{+}CD11b^{+}F4/80^{+}iNOS^{-}CD206^{+}$ for M2 macrophages. Stained cells were analyzed on an Attune NxT flow cytometer (Thermo Fisher Scientific). Data were analyzed using Flow Jo 10.6 software (BD Biosciences, NJ, USA).

Co-Immunoprecipitation (Co-IP)

Pancreatic tissue lysates were prepared using weak RIPA lysis buffer (P0013D; Beyotime) containing protease and phosphatase inhibitors followed by 15 min centrifugation at 10,000×*g*, 4 °C. For Co-IP, the crude whole-cell extract was incubated with the antibody at 4 °C overnight. Then, 100 μL prewashed Protein A + G Agarose (P2078-1; Beyotime) was added to the mixture and incubated at 4 °C for 4 h with gentle agitation. After extensive washing with weak RIPA buffer, the interacting proteins were eluted with SDS buffer and analyzed by immunoblotting. Dilution ratios of antibodies were as follows: STAT3 (1:50), SIRT1 (1:30), and pan Acetyl-lysine (1:50).

Statistics

Data were expressed as mean ± SD. For flow cytometry statistics analyses, data were expressed as median ± interquartile range. $P < 0.05$ was considered statistically significant. The difference among three or more groups was determined using a one-way ANOVA followed by Tukey's *post hoc* test. All data were analyzed using GraphPad Prism 8 software (CA, USA).

RESULTS

(*R*)-TML104 mitigates pancreatic damage in the experimental AP model

To investigate the dose-dependent effect of (*R*)-TML104 (structure in Fig. 1a) on experimental AP, mice were treated with three doses of (*R*)-TML104 (5, 10, and 20 mg·kg^{-1}) before caerulein stimulation. We found that (*R*)-TML104 exerted the optimal inhibitory effects on caerulein-induced pancreatic edema, serum amylase levels, serum lipase levels, and pancreatic MPO activities at 20 mg·kg^{-1},

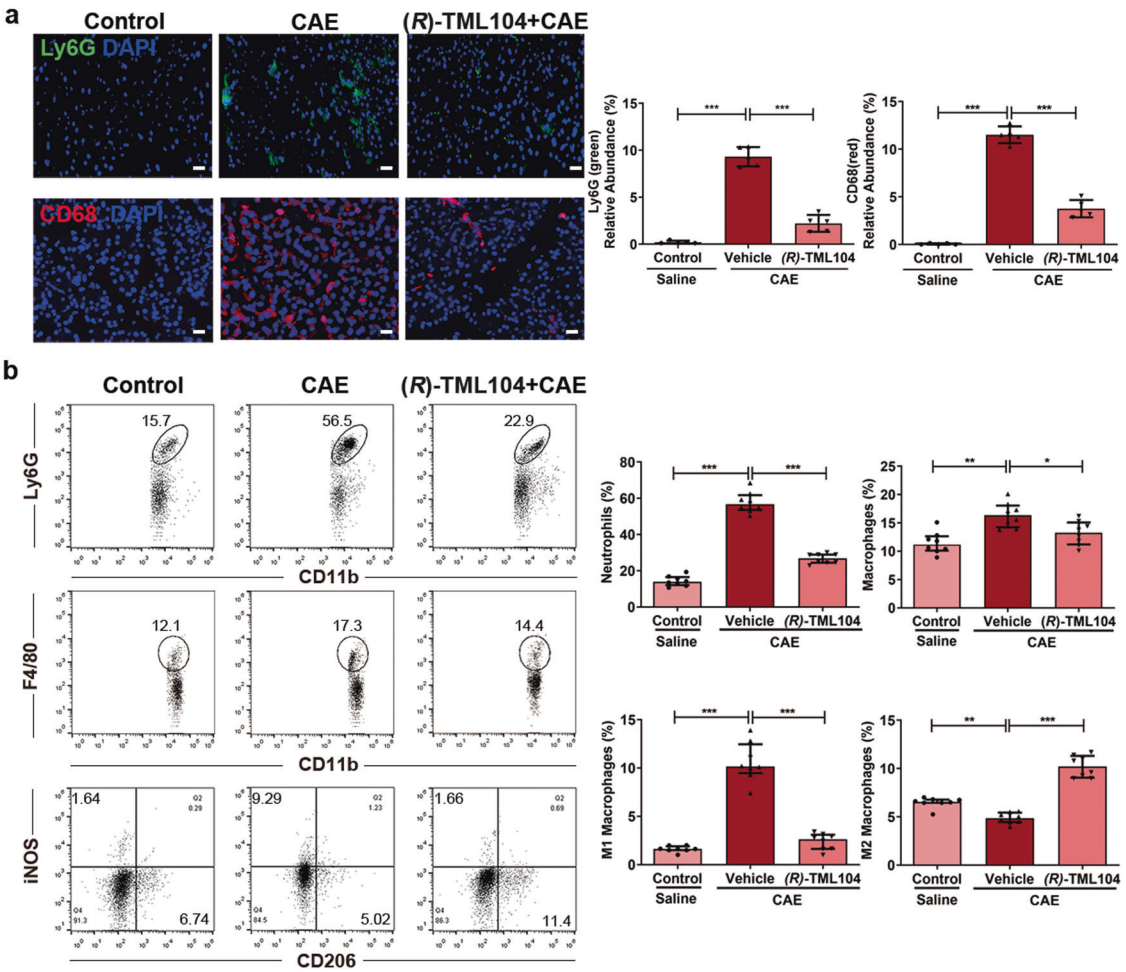

Fig. 2 (*R*)-TML104 suppresses caerulein-induced immune cell imbalance. a Localization and expression of Ly6G (green) and CD68 (red) in the pancreas by immunofluorescent staining. Nuclei were stained with DAPI (blue). Scale bar: 50 μm. **b** The frequencies of $Ly6G^+$ neutrophils among $CD45^+CD11b^+$ population, $F4/80^+$ macrophages among $CD45^+CD11b^+$ population, $iNOS^+CD206^-$ M1 macrophages among $CD45^+CD11b^+F4/80^+$ population and $iNOS^-CD206^+$ M2 macrophages among $CD45^+CD11b^+F4/80^+$ population in the pancreas were shown by flow cytometry. Data (**a**) were representative and were mean ± SD ($n = 5$). Data (**b**) were representative and were median ± interquartile range ($n = 8$). $^*P < 0.05$, $^{**}P < 0.01$, $^{***}P < 0.001$.

and thus this dose was used for subsequent experiments (Fig. S1a–d). Treatment with resveratrol alleviated the degeneration, leukocyte infiltration, and pancreatic edema in mice with AP [20, 21]. (*R*)-TML104 and resveratrol both exerted protective effects on the severity of AP, as evidenced by reduced pancreatic edema, serum amylase levels, serum lipase levels, and pancreatic MPO activities (Fig. 1b–e). Furthermore, the histological examination of pancreatic sections confirmed an overall improved disease severity index in (*R*)-TML104-treated and resveratrol-treated mice. Pancreatic edema, inflammatory cell infiltration, and necrosis were reduced following treatment with (*R*)-TML104 or resveratrol (Fig. 1f). Notably, (*R*)-TML104 exerted a more obvious beneficial effect on pancreatic edema, serum lipase levels, and pancreatic histology than resveratrol at the same dosage. Meanwhile, (*R*)-TML104 alone did not cause any difference in all AP markers compared with the control group. Taken together, (*R*)-TML104 alleviates pancreatic injury in mice with AP, without adverse effects.

(*R*)-TML104 suppresses caerulein-induced imbalance of immune cells

The dysregulated infiltration of innate immune cells, including neutrophils and macrophages, is a key pathophysiological event in AP development [9]. Neutrophils and macrophages were identified by performing immunofluorescence staining for Ly6G and CD68 respectively. The numbers of pancreatic Ly6G-positive neutrophils and CD68-positive macrophages decreased significantly following (*R*)-TML104 treatment (Fig. 2a). Macrophages can polarize into classically activated macrophages (M1) with proinflammatory properties and alternatively activated macrophages (M2) with anti-inflammatory properties in response to the microenvironment signals [30]. Furthermore, the frequencies of neutrophils and the polarization of macrophages in the pancreas were determined using flow cytometry. Caerulein caused the robust increases in the frequencies of neutrophils ($CD45^+CD11b^+Ly6G^+$), macrophages ($CD45^+CD11b^+F4/80^+$), and M1 macrophages ($CD45^+CD11b^+F4/80^+iNOS^+CD206^-$) (Fig. 2b) in the pancreas. Intriguingly, (*R*)-TML104 administration mitigated the increases in neutrophils, macrophages, and M1 macrophages and simultaneously promoted macrophage polarization to M2 macrophages ($CD45^+CD11b^+F4/80^+iNOS^-CD206^+$) (Fig. 2b). Collectively, these data suggest that (*R*)-TML104 inhibits caerulein-induced immune cell dysregulation by reducing the frequencies of neutrophils and macrophages and modulating macrophage phenotypes.

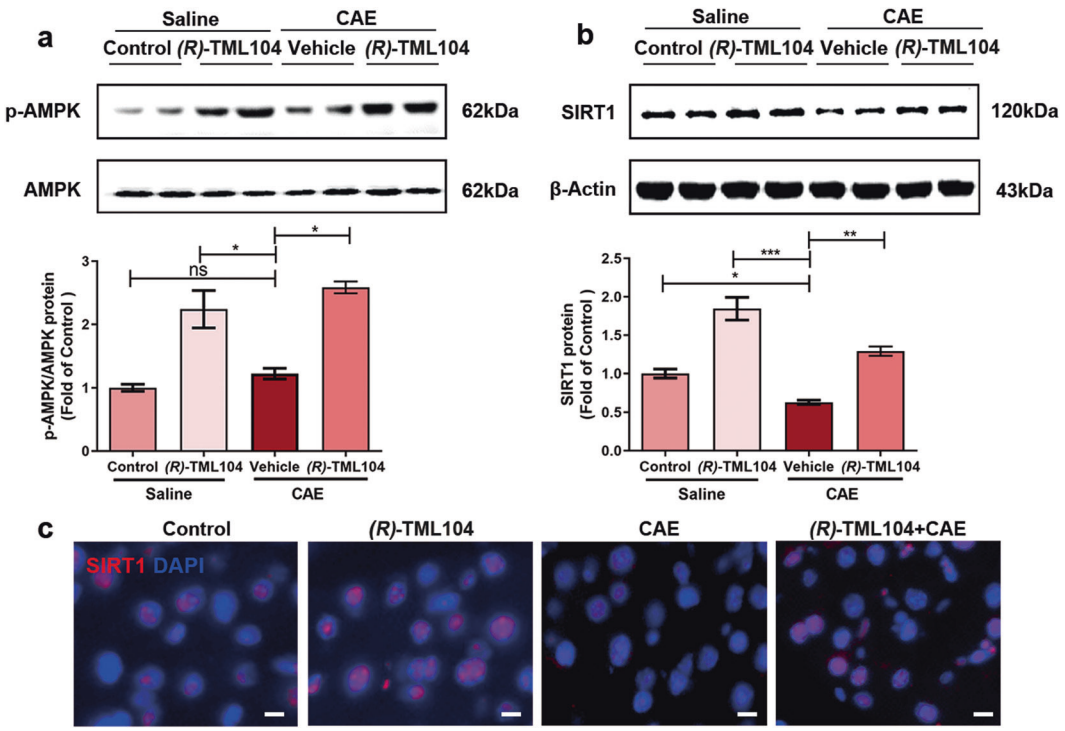

Fig. 3 (*R*)-TML104 upregulates pancreatic SIRT1 expression. **a** Western blot and densitometry analyses of p-AMPK and AMPK in the pancreas. **b** Western blot and densitometry analyses of SIRT1 and β-Actin in the pancreas. **c** Localization and expression of SIRT1 (red) in the pancreas by immunofluorescent staining. Nuclei were stained with DAPI (blue). Scale bar: 20 μm. Data (**a**), (**b**) were representative and were mean ± SD from six independent mice. Data (**c**) were representative of six independent mice. $^{*}P < 0.05$, $^{**}P < 0.01$, $^{***}P < 0.001$

(*R*)-TML104 upregulates pancreatic SIRT1 expression

Resveratrol plays an important role in inflammation by activating the AMP-activated protein kinase (AMPK)-SIRT1 pathway [31]. Therefore, we investigated the phosphorylation of AMPK and the expression of SIRT1. (*R*)-TML104 stimulated AMPK phosphorylation and upregulated SIRT1 expression in the pancreas (Fig. 3a, b). In addition, the upregulation of pancreatic SIRT1 expression by (*R*)-TML104 was also identified using immunofluorescence staining (Fig. 3c). Together, the protective effect of (*R*)-TML104 on experimental AP may be mediated through upregulation of SIRT1.

(*R*)-TML104 inhibits the activation of STAT3 by modulating the interaction between STAT3 and SIRT1

The inflammatory factors IL-6, CCL2, and MIP-2, associated with neutrophils and macrophages, are recognized to be mediators of AP [1, 12, 32]. Next, we investigated the effect of (*R*)-TML104 on inflammatory cytokine levels. (*R*)-TML104 alleviated AP-induced increases in pancreatic IL-6, CCL2, and MIP-2 levels (Fig. 4a). In addition, the inhibitory effects of (*R*)-TML104 on the chemokines CCL2 and MIP-2 were determined by performing immunofluorescence staining of pancreatic tissues. (Fig. 4b). Activation of the IL-6-STAT3 pathway is responsible for pancreatic CCL2 and MIP-2 expression during AP [13, 15]. We found that STAT3 phosphorylation was suppressed by (*R*)-TML104 (Fig. 4c). STAT3 requires acetylation to exert its transcriptional function and SIRTI affects its acetylation [13, 33]. Interestingly, (*R*)-TML104 enhanced the effect of SIRT1 on the deacetylation of STAT3, as evidenced by Co-IP (Fig. 4d). These data confirm that (*R*)-TML104 treatment reduces the activation of the IL-6-STAT3 pathway and induces the interaction of SIRT1 and STAT3.

SIRT1 inhibition abolishes (*R*)-TML104-exerted protective effects on pancreatic damage

Next, the specific SIRT1 inhibitor EX527 was administered before caerulein-induced AP to block SIRT1 activity. EX527 abolished (*R*)-TML104-exerted protective effects on caerulein-induced pancreatic damage, as evidenced by increased pancreatic edema, serum amylase levels, serum lipase levels, and pancreatic MPO activities (Fig. 5a–d). Furthermore, the histological examination confirmed that the protective effect of (*R*)-TML104 on pancreatic injury and necrosis was also blocked by EX527 (Fig. 5e). In addition, EX527 blocked the inhibitory effects of (*R*)-TML104 on pancreatic production of IL-6, CCL2, and MIP-2 (Fig. 6a, b). Consistent with inflammatory cytokine expression, EX527 reversed (*R*)-TML104-exerted decreases in the frequencies of neutrophils, macrophages, and M1 macrophages and increases in the frequency of M2 macrophages (Fig. 6c). Moreover, EX527 abrogated the modulatory effects of (*R*)-TML104 on STAT3 activation and the SIRT1-STAT3 interaction (Fig. 6d, e). Together, these results demonstrate that (*R*)-TML104 exerts its anti-inflammatory effects by upregulating SIRT1 and inhibiting STAT3 acetylation.

DISCUSSION

Our study indicates that (*R*)-TML104 exerts protective effects on the development of caerulein-induced AP. It alleviates the severity of AP by attenuating pancreatic damage, inhibiting IL-6-STAT3 signaling pathway activation, reducing levels of the proinflammatory chemokines CCL2 and MIP-2, and modulating pancreatic infiltration of neutrophils and macrophages. Importantly, (*R*)-TML104 mitigates attenuation of AP by suppressing the acetylation of STAT3 via SIRT1 (Fig. 7).

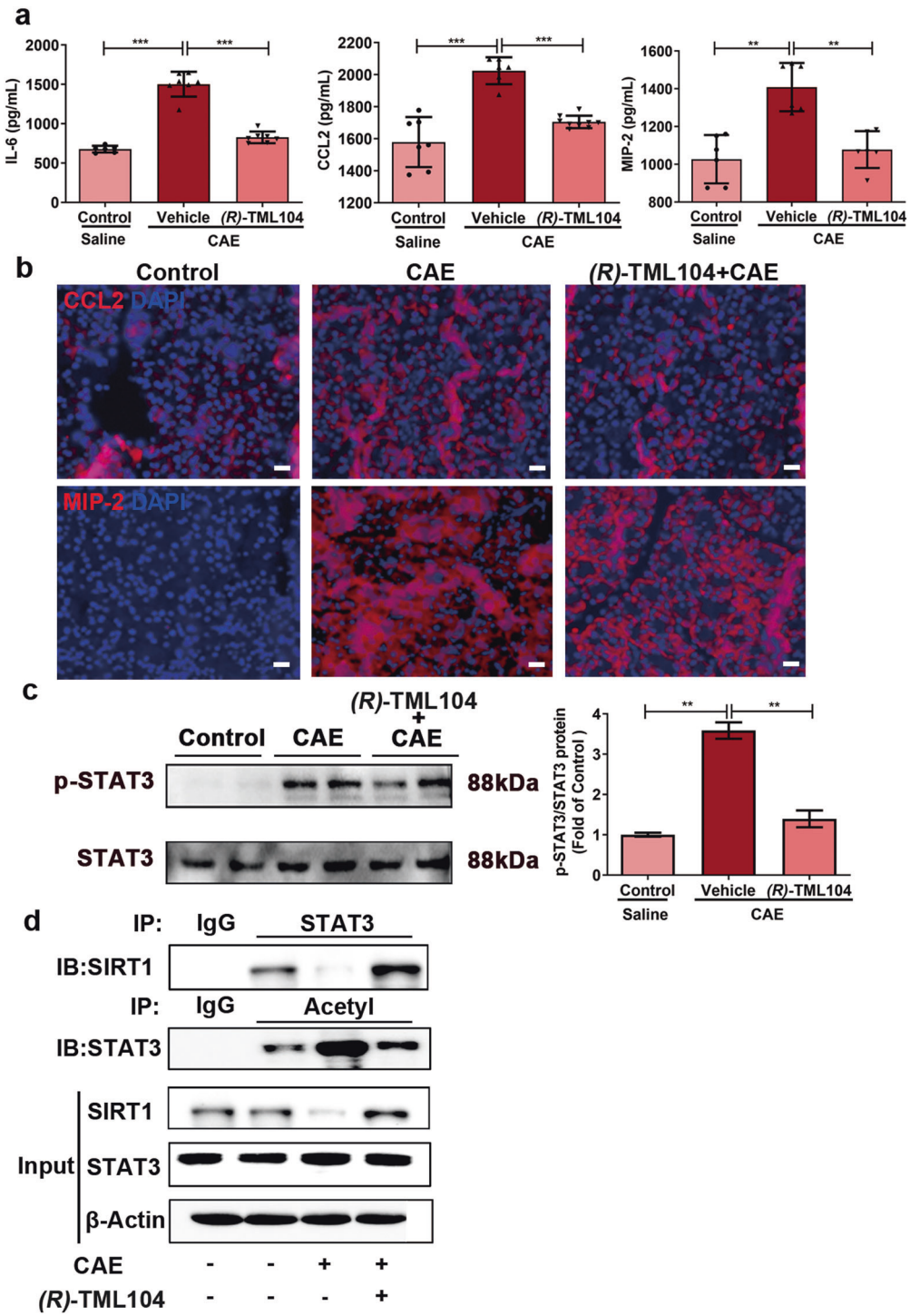

Fig. 4 **(*R*)-TML104 inhibits activation of STAT3 through modulation of the interaction between STAT3 and SIRT1. a** Pancreatic IL-6, CCL2, and MIP-2 levels were determined by ELISA. **b** Localization and expression of CCL2 (red) and MIP-2 (red) in the pancreas by immunofluorescent staining. Nuclei were stained with DAPI (blue). Scale bar: 50 μm. **c** Western blot and densitometry analyses of p-STAT3 and STAT3 in the pancreas. **d** Co-IP analyses of SIRT1-STAT3 and STAT3-pan Acetyl-lysine interactions in the pancreas. Data (**a**) were the mean ± SD ($n = 6–9$). Data (**b**), (**d**) were representative of six independent mice. Data (**c**) were representative and were mean ± SD from six independent mice. $^{**}P < 0.01$, $^{***}P < 0.001$.

STATs are critical mediators of functional responses in cytokine signaling [13, 34]. Different STATs are activated by distinct groups of cytokines. STAT3 is activated by IL-6 family members [14, 35]. STAT3 is the most prominent member of all STATs and has been established as a major proinflammatory protein [13]. Many studies have reported a vital role for STAT3 in AP [15, 27]. Inhibiting the activation of STAT3 is a promising therapeutic approach for AP. STAT3 activation is regulated, either positively or negatively, by different post-translational mechanisms including serine or tyrosine

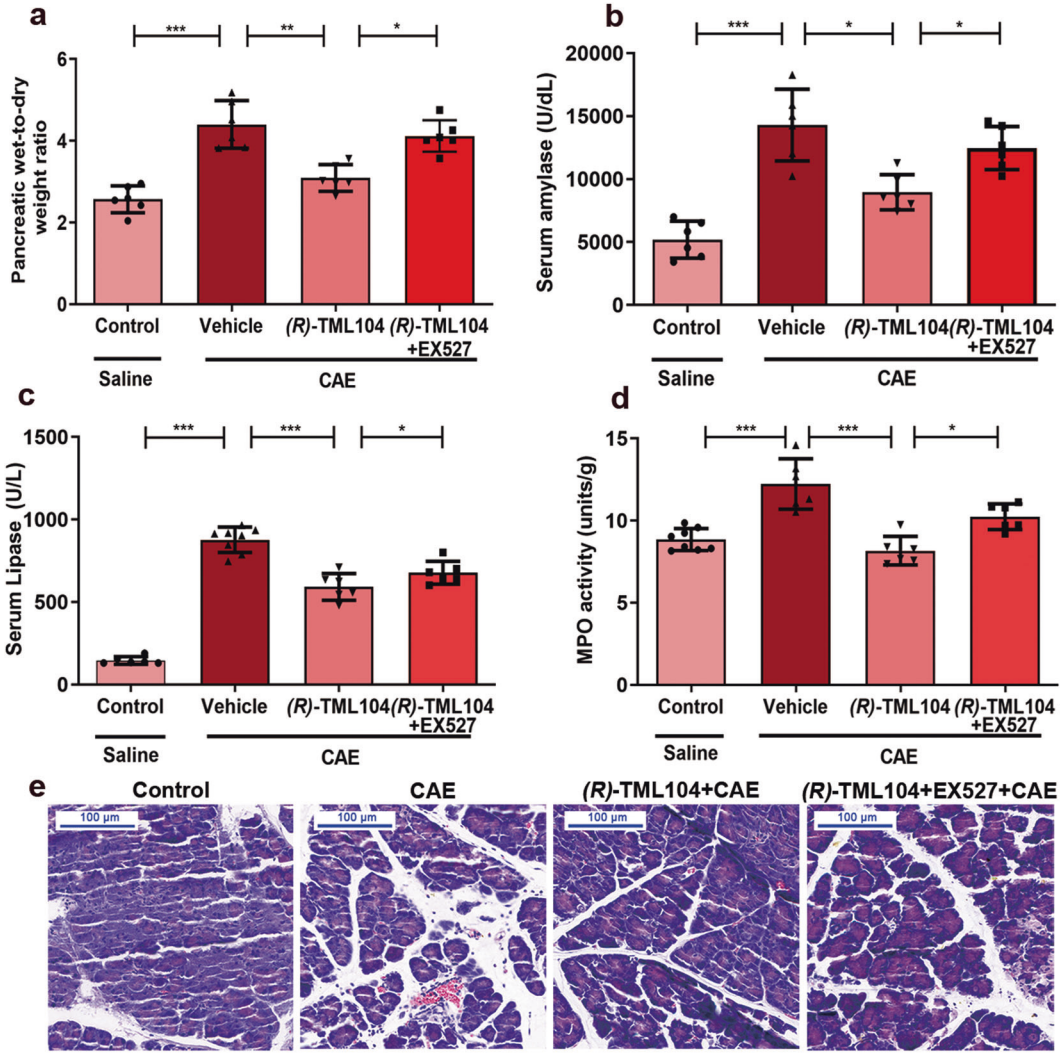

Fig. 5 SIRT1 is momentous for (*R*)-TML104 to inhibit caerulein-induced AP. a Pancreatic wet-to-dry weight ratio. **b** Serum amylase levels. **c** Serum lipase levels. **d** Pancreatic MPO activities. **e** Representative images of pancreatic damage by H&E staining. Scale bar: 100 μm. Data (**a**)–(**d**) were the mean ± SD ($n = 6$–8). Data (**e**) were representative of six independent mice. $^{*}P < 0.05$, $^{**}P < 0.01$, $^{***}P < 0.001$

phosphorylation, acetylation, or demethylation [36]. The nuclear translocation of STAT3 and its subsequent activation of target genes depends on dimerization [16]. Tyrosine phosphorylation has long been considered to play a central role in STAT3 dimerization. However, some studies have suggested that phosphorylation is not necessary for STAT3 dimerization [37]. Notably, reversible acetylation might modulate STAT3 dimerization and phosphorylation [36, 38]. Accumulating evidence has indicated that acetylation of STAT3 enhances DNA binding, transactivation activity, and nuclear localization and is involved in many signaling pathways [39]. More importantly, to date, little research has been conducted on the acetylation of STAT3 in AP.

The acetylation/deacetylation of STAT3 is precisely regulated by histone acetyltransferases and deacetylase [40]. STAT3 acetylation relies on a balance between acetylation activated by p300 acetylase and deacetylation modulated by histone deacetylase (HDAC) enzymes [16]. SIRT1, the best-characterized member of class III HDACs, mediates the deacetylation of STAT3. The modulatory effect of SIRT1 on different cellular processes, particularly inflammation, is largely mediated by limiting STAT3 acetylation [41]. It has been demonstrated that SIRT1 activation impedes proinflammatory cytokine expression and T helper cell 17 development via STAT3 deacetylation [42]. Resveratrol is a classical activator of SIRT1. The inhibition of SIRT1 deacetylation depends on nicotinamide adenine dinucleotide^{+} (NAD^{+}). Resveratrol lowers the Michaelis constant of SIRT1 for both the acetylated substrate and NAD^{+} and increases cell survival by stimulating SIRT1-dependent deacetylation [43].

Resveratrol is a polyphenol that has been shown to possess multiple beneficial properties, such as antiaging, antioxidant, and anti-inflammatory activities [18]. The antioxidant and immunomodulatory properties of resveratrol may represent a promising chemopreventive approach for AP prevention [23]. Numerous studies have reported that resveratrol effectively inhibits the progression of AP in vivo and in vitro, and a clinical trial has also been designed to reveal its undeniable therapeutic value in AP [22, 44]. However, resveratrol is easily absorbed and rapidly metabolized, mainly as sulfo- and glucuro-conjugates which are excreted in urine [25]. Many studies have focused on improving its bioavailability and regulatory function. One strategy is to create derivatives that

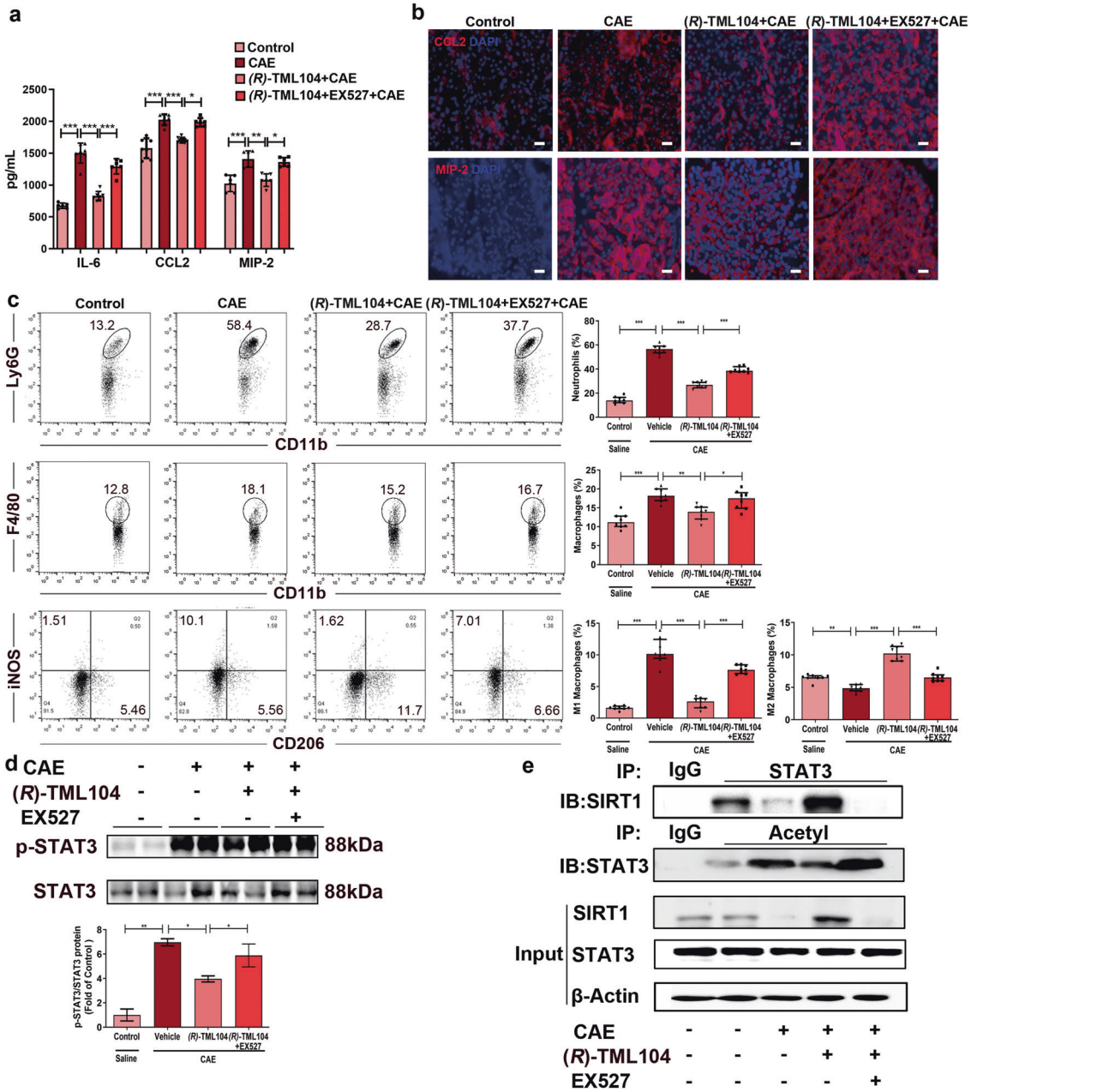

Fig. 6 SIRT1 inhibition abolishes (*R*)-TML104-exerted protective effects on pancreatic damage. a Pancreatic IL-6, CCL2, and MIP-2 levels were determined by ELISA. **b** Localization and expression of CCL2 (red) and MIP-2 (red) in the pancreas by immunofluorescent staining. Nuclei were stained with DAPI (blue). Scale bar: 50 μm. **c** The frequencies of Ly6G$^+$ neutrophils among CD45$^+$CD11b$^+$ population, F4/80$^+$ macrophages among CD45$^+$CD11b$^+$ population, iNOS$^+$CD206$^-$ M1 macrophages among CD45$^+$CD11b$^+$F4/80$^+$ population and iNOS$^-$CD206$^+$ M2 macrophages among CD45$^+$CD11b$^+$F4/80$^+$ population in the pancreas were shown by flow cytometry. **d** Western blot and densitometry analyses of p-STAT3 and STAT3 in the pancreas. **e** Co-IP analyses of SIRT1-STAT3 and STAT3-pan acetyl-lysine interactions in the pancreas. Data (**a**) were the mean ± SD ($n = 6$-9). Data (**b**) and (**e**) were representative of six independent mice. Data (**c**) were representative and were median ± interquartile range ($n = 8$). Data (**d**) were representative and were mean ± SD from six independent mice. *$P < 0.05$, **$P < 0.01$, ***$P < 0.001$.

optimize the structure of resveratrol. Here, we synthesized a novel resveratrol analog (*R*)-TML104 with improved structural stability, compared with resveratrol. In addition, (*R*)-TML104, similar to resveratrol, possessed the ability to induce SIRT1 production. Furthermore, using the same administration route and dose, (*R*)-TML104 exerted a better inhibitory effect on pancreatic damage and inflammation than resveratrol in mice with AP.

Collectively, our data demonstrate that the resveratrol analog (*R*)-TML104 attenuates pancreatic damage and associated inflammatory cell infiltration during AP by increasing SIRT1 expression and subsequently suppressing STAT3 acetylation. Importantly, (*R*)-TML104 exerts a better inhibitory effect on AP than resveratrol. Finally, our study supports the use of the novel resveratrol analog (*R*)-TML104 as the SIRT1/STAT3 axis regulator, hence preventing the development of AP.

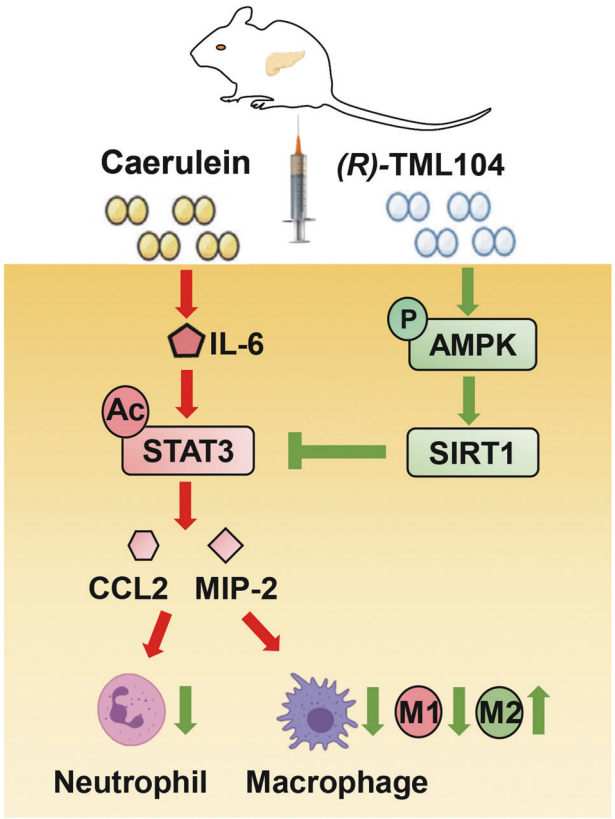

Fig. 7 A schematic representation of the modulatory effects of (*R*)-TML104 on inflammatory pathways during AP. Caerulein induces the activation of the IL-6-STAT3 pathway and inflammation in mice. (*R*)-TML104 upregulates the SIRT1 expression and SIRT1-mediated the deacetylation of STAT3. Hence, (*R*)-TML104 protects pancreatic tissue against damage and the subsequent inflammatory responses in a SIRT1-dependent manner.

DATA AVAILABILITY

The authors declare that the main data supporting the findings of this study are available within the article. Extra data are available from the corresponding author upon request.

ACKNOWLEDGEMENTS

The work was supported by funds from the National Natural Science Foundation of China (Grant nos: 80270666, 81870439, 81973322, 91642114, 31570915, and National Youth 1000 Talents Plan), the Natural Science Foundation for Distinguished Young Scholars of Jiangsu Province (Grant no: BK20200026), Jiangsu Province Recruitment Plan for High-level, Innovative and Entrepreneurial Talents (Innovative Research Team), Wuxi Social Development Funds for International Science & Technology Cooperation (Grant no: WX0303B010518180007PB), Jiangsu Province "Six Summit Talents" program (Grant no: YY-038), Jiangsu Province Qing Lan Project, National First-class Discipline Program of Food Science and Technology (Grant no: JUFSTR20180103), the Fundamental Research Funds for the Central Universities (Grant nos: JUSRP221037, JUSRP22007), Postgraduate Research & Practice Innovation Program of Jiangsu Province (Grant no: KYCX20_1876), Collaborative Innovation Center of Food Safety and Quality Control in Jiangsu Province and Wuxi Taihu Talent Project. Shanghai Municipal Committee of Science and Technology (Grant no: 17JC1400200). Youth Project of Public Health Research Center of Jiangnan University (Grant no: JUPH201825); Translational Medicine Project of Wuxi Municipal Commission of Health and Family Planning (Grant no: ZM007); Wuxi City's first "double hundred" young and middle-aged medical and health talents (Grant no: BJ2020045); Wuxi Social Development Science and Technology Demonstration Project (Grant no: N20201003).

AUTHOR CONTRIBUTIONS

ZNR, MYZ, YH, and DXS performed experiments and analyzed data. XS synthesized and provided novel resveratrol analog (*R*)-TML104. JS and LLP designed and interpreted experiments. JY contributed to the data acquisition and critically reviewed the manuscript. ZNR, LLP, and JS wrote the paper.

ADDITIONAL INFORMATION

Supplementary information The online version contains supplementary material available at https://doi.org/10.1038/s41401-021-00744-y.

Competing interests: The authors disclose no competing interests.

REFERENCES

1. Lankisch PG, Apte M, Banks PA. Acute pancreatitis. Lancet. 2015;386:85–96.
2. Saluja AK, Lerch MM, Phillips PA, Dudeja V. Why does pancreatic overstimulation cause pancreatitis? Annu Rev Physiol. 2007;69:249–69.
3. Logsdon CD, Ji B. The role of protein synthesis and digestive enzymes in acinar cell injury. Nat Rev Gastroenterol Hepatol. 2013;10:362–70.
4. Frossard J-L, Steer ML, Pastor CM. Acute pancreatitis. Lancet. 2008;371:143–52.
5. Mayerle J, Sendler M, Hegyi E, Beyer G, Lerch MM, Sahin-Tóth M. Genetics, cell biology, and pathophysiology of pancreatitis. Gastroenterology. 2019;156:1951–68.
6. Steinberg W, Tenner S. Acute pancreatitis. N Engl J Med. 1994;330:1198–210.
7. Merza M, Hartman H, Rahman M, Hwaiz R, Zhang E, Renström E, et al. Neutrophil extracellular traps induce trypsin activation, inflammation, and tissue damage in mice with severe acute pancreatitis. Gastroenterology. 2015;149:1920–31.
8. Sendler M, Weiss F-U, Golchert J, Homuth G, van den Brandt C, Mahajan UM, et al. Cathepsin B-mediated activation of trypsinogen in endocytosing macrophages increases severity of pancreatitis in mice. Gastroenterology. 2018;154:704–18.
9. Watanabe T, Kudo M, Strober W. Immunopathogenesis of pancreatitis. Mucosal Immunol. 2017;10:283–98.
10. Saeki K, Kanai T, Nakano M, Nakamura Y, Miyata N, Sujino T, et al. CCL2-induced migration and SOCS3-mediated activation of macrophages are involved in cerulein-induced pancreatitis in mice. Gastroenterology. 2012;142:1010–20.
11. Han X, Li B, Ye X, Mulatibieke T, Wu J, Dai J, et al. Dopamine D receptor signalling controls inflammation in acute pancreatitis via a PP2A-dependent Akt/NF-κB signalling pathway. Br J Pharmacol. 2017;174:4751–70.
12. Pan X, Fang X, Wang F, Li H, Niu W, Liang W, et al. Butyrate ameliorates caerulein-induced acute pancreatitis and associated intestinal injury by tissue-specific mechanisms. Br J Pharmacol. 2019;176:4446–61.
13. Yu H, Pardoll D, Jove R. STATs in cancer inflammation and immunity: a leading role for STAT3. Nat Rev Cancer. 2009;9:798–809.
14. Zhang H, Neuhöfer P, Song L, Rabe B, Lesina M, Kurkowski MU, et al. IL-6 trans-signaling promotes pancreatitis-associated lung injury and lethality. J Clin Invest. 2013;123:1019–31.
15. Lesina M, Wörmann SM, Neuhöfer P, Song L, Algül H. Interleukin-6 in inflammatory and malignant diseases of the pancreas. Semin Immunol. 2014;26:80–7.
16. Yuan Z-L, Guan Y-J, Chatterjee D, Chin YE. Stat3 dimerization regulated by reversible acetylation of a single lysine residue. Science. 2005;307:269–73.
17. Xia N, Daiber A, Förstermann U, Li H. Antioxidant effects of resveratrol in the cardiovascular system. Br J Pharmacol. 2017;174:1633–46.
18. Rauf A, Imran M, Butt MS, Nadeem M, Peters DG, Mubarak MS. Resveratrol as an anti-cancer agent: a review. Crit Rev Food Sci Nutr. 2018;58:1428–47.
19. Hubbard BP, Sinclair DA. Small molecule SIRT1 activators for the treatment of aging and age-related diseases. Trends Pharmacol Sci. 2014;35:146–54.
20. Wang N, Zhang F, Yang L, Zou J, Wang H, Liu K, et al. Resveratrol protects against L-arginine-induced acute necrotizing pancreatitis in mice by enhancing SIRT1-mediated deacetylation of p53 and heat shock factor 1. Int J Mol Med. 2017;40:427–37.
21. Liu D, Song G, Ma Z, Geng X, Dai Y, Yang T, et al. Resveratrol improves the therapeutic efficacy of bone marrow-derived mesenchymal stem cells in rats with severe acute pancreatitis. Int Immunopharmacol. 2020;80:106128.
22. Xiang H, Zhang Q, Qi B, Tao X, Xia S, Song H, et al. Chinese herbal medicines attenuate acute pancreatitis: pharmacological activities and mechanisms. Front Pharmacol. 2017;8:216.
23. Agah S, Akbari A, Sadeghi E, Morvaridzadeh M, Basharat Z, Palmowski A, et al. Resveratrol supplementation and acute pancreatitis: a comprehensive review. Biomed Pharmacother. 2021;137:111268.
24. Walle T. Bioavailability of resveratrol. Ann N Y Acad Sci. 2011;1215:9–15.
25. Cottart CH, Nivet-Antoine V, Laguillier-Morizot C, Beaudeux JL. Resveratrol bioavailability and toxicity in humans. Mol Nutr Food Res. 2010;54:7–16.
26. Percie du Sert N, Hurst V, Ahluwalia A, Alam S, Avey MT, Baker M, et al. The ARRIVE guidelines 2.0: Updated guidelines for reporting animal research. Br J Pharmcol. 2020;177:3617–24.

27. Ren Z, Li H, Zhang M, Zhao Y, Fang X, Li X, et al. A novel derivative of the natural product danshensu suppresses inflammatory responses to alleviate caerulein-induced acute pancreatitis. Front Immunol. 2018;9:2513.
28. Tsang SW, Guan YF, Wang J, Bian ZX, Zhang HJ. Inhibition of pancreatic oxidative damage by stilbene derivative dihydro-resveratrol: implication for treatment of acute pancreatitis. Sci Rep. 2016;6:22859.
29. Smith MR, Syed A, Lukacsovich T, Purcell J, Barbaro BA, Worthge SA, et al. A potent and selective Sirtuin 1 inhibitor alleviates pathology in multiple animal and cell models of Huntington's disease. Hum Mol Genet. 2014;23:2995–3007.
30. Hu F, Lou N, Jiao J, Guo F, Xiang H, Shang D. Macrophages in pancreatitis: mechanisms and therapeutic potential. Biomed Pharmacother. 2020;131:110693.
31. Price NL, Gomes AP, Ling AJY, Duarte FV, Martin-Montalvo A, North BJ, et al. SIRT1 is required for AMPK activation and the beneficial effects of resveratrol on mitochondrial function. Cell Metab. 2012;15:675–90.
32. Ramnath RD, Sun J, Bhatia M. Role of calcium in substance P-induced chemokine synthesis in mouse pancreatic acinar cells. Br J Pharmacol. 2008;154:1339–48.
33. Nie Y, Erion DM, Yuan Z, Dietrich M, Shulman GI, Horvath TL, et al. STAT3 inhibition of gluconeogenesis is downregulated by SirT1. Nat Cell Biol. 2009;11:492–500.
34. Wang Y, Shen Y, Wang S, Shen Q, Zhou X. The role of STAT3 in leading the crosstalk between human cancers and the immune system. Cancer Lett. 2018;415:117–28.
35. Johnson DE, O'Keefe RA, Grandis JR. Targeting the IL-6/JAK/STAT3 signalling axis in cancer. Nat Rev Clin Oncol. 2018;15:234–48.
36. Stark GR, Darnell JE. The JAK-STAT pathway at twenty. Immunity. 2012;36:503–14.
37. Braunstein J, Brutsaert S, Olson R, Schindler C. STATs dimerize in the absence of phosphorylation. J Biol Chem. 2003;278:34133–40.
38. Ma L, Gao J-S, Guan Y, Shi X, Zhang H, Ayrapetov MK, et al. Acetylation modulates prolactin receptor dimerization. Proc Natl Acad Sci USA. 2010;107:19314–9.
39. Wang R, Cherukuri P, Luo J. Activation of Stat3 sequence-specific DNA binding and transcription by p300/CREB-binding protein-mediated acetylation. J Biol Chem. 2005;280:11528–34.
40. O'Shea JJ, Kanno Y, Chen X, Levy DE. Cell signaling. Stat acetylation–a key facet of cytokine signaling? Science. 2005;307:217–8.
41. Chang H-C, Guarente L. SIRT1 and other sirtuins in metabolism. Trends Endocrinol Metab. 2014;25:138–45.
42. Limagne E, Thibaudin M, Euvrard R, Berger H, Chalons P, Végan F, et al. Sirtuin-1 activation controls tumor growth by impeding Th17 differentiation via STAT3 deacetylation. Cell Rep. 2017;19:746–59.
43. Howitz KT, Bitterman KJ, Cohen HY, Lamming DW, Lavu S, Wood JG, et al. Small molecule activators of sirtuins extend *Saccharomyces cerevisiae* lifespan. Nature. 2003;425:191–6.
44. Tarasiuk A, Fichna J. Effectiveness and therapeutic value of phytochemicals in acute pancreatitis: a review. Pancreatology. 2019;19:481–7.